Frontiers in Bioscience Landmark

Front. Biosci. (Landmark Ed) **2025**; 30(12): 46724
https://doi.org/10.31083/FBL46724

Original Research

Ginkgolide B Promotes Angiogenesis After Oxygen-Glucose Deprivation by Regulating AKT1 in bEnd.3 Cells

Yuanchen Liao[1,†], Lei Luo[1,†], Qiang Ma[2,3], Siyang Yan[2], Menghao He[1], Lijuan Liu[2], Xiaofeng Gao[2], Desheng Zhou[2,*], Yao Chen[2,*]

[1]The First School of Clinical Chinese Medicine, Hunan University of Chinese Medicine, 410208 Changsha, Hunan, China
[2]Department of Neurology, The First Affiliated Hospital of Hunan University of Chinese Medicine, 410006 Changsha, Hunan, China
[3]The Key Laboratory of Hunan Province for Integrated Traditional Chinese and Western Medicine on Prevention and Treatment of Cardio-Cerebral Diseases, College of Integrated Traditional Chinese and Western Medicine, Hunan University of Chinese Medicine, 410208 Changsha, Hunan, China
*Correspondence: zds1101@foxmail.com (Desheng Zhou); cy45637@163.com (Yao Chen)
†These authors contributed equally.
Academic Editor: Gabriella Lupo
Submitted: 18 September 2025 Revised: 1 November 2025 Accepted: 13 November 2025 Published: 15 December 2025

Abstract

Background: Ischemic stroke leads to significant neuronal damage, and impaired angiogenesis remains a critical factor limiting post-stroke recovery. Ginkgolide B (GB), a key component of Ginkgo biloba extract, has shown potential neuroprotective effects, but its pro-angiogenic mechanisms remain unclear. **Methods**: To investigate the effects of GB, we established an oxygen–glucose deprivation/reperfusion (OGD/R) model using bEnd.3 cells. Potential molecular targets of GB were explored through a combination of network pharmacology analysis, protein–protein interaction (PPI) network construction, pathway enrichment, and molecular dynamics simulations. Based on these predictions, a series of *in vitro* assays—including Cell Counting Kit-8 (CCK-8), 5-ethynyl-2′-deoxyuridine (EdU) incorporation, wound-healing, Transwell migration, and Matrigel tube formation tests—were performed to evaluate cell viability, proliferation, migration, and angiogenic activity. Western blotting was conducted to detect AKT serine/threonine kinase 1 (AKT1), vascular endothelial growth factor (VEGF), and Angiogenin (Ang) expression and clarify the role of the AKT1/VEGF/Ang pathway. **Results**: Bioinformatics analysis identified 19 potential targets, among which AKT1, Matrix Metalloproteinase 9 (MMP9), and Prostaglandin-Endoperoxide Synthase 2 (PTGS2) exhibited the highest relevance. GB showed no evident cytotoxicity at concentrations up to 40 μM and mitigated the OGD/R-induced reduction in cell viability. At this concentration range, GB also enhanced endothelial proliferation, migration, and tube formation in bEnd.3 cells. Mechanistic studies revealed that MK2206 inhibition of AKT1 markedly suppressed AKT1 expression ($p < 0.01$), impaired angiogenic capacity, and aggravated ischemic–hypoxic injury, whereas GB treatment significantly increased VEGF and Ang expression ($p < 0.01$), likely via AKT1 upregulation ($p < 0.01$). **Conclusion**: GB promotes angiogenesis and exerts neuroprotective effects by activating the AKT1/VEGF/Ang signaling pathway, suggesting its potential therapeutic value for ischemic stroke–related injuries.

Keywords: Ginkgolide B; ischemic stroke; angiogenesis; AKT1

1. Introduction

Ischemic stroke (IS) is a common and severe neurological disorder caused by impaired cerebral blood flow, resulting in localized ischemic–hypoxic necrosis and subsequent neurological deficits [1]. It is the primary cause of long-term disability and ranks second among global causes of death [2]. The sustained deprivation of oxygen and nutrients results in neuronal injury, which constitutes the key pathological feature of IS. Collateral circulation serves as an important compensatory mechanism that helps restore regional perfusion and oxygen supply, thereby improving clinical outcomes [3]. Angiogenesis, a principal component of tertiary collateral circulation, drives the formation of new microvessels from existing vasculature. This process supports the ischemic penumbra by providing oxygen and nutrients, thus promoting repair after ischemic injury [4,5]. Both clinical and experimental studies have shown that enhanced angiogenesis contributes to tissue recovery, vascular remodeling, and improved perfusion in peri-infarct regions, ultimately facilitating neurological restoration [6–8]. For these reasons, promoting post-ischemic angiogenesis has emerged as a potential therapeutic strategy to improve outcomes after cerebral infarction [9–11]. In particular, early and robust angiogenic responses can stabilize local blood flow, limit neuronal loss, and reduce neurological deficits in the acute phase [12,13].

Traditional Chinese medicine (TCM) has gained attention in recent years for its potential in preventing and treating cardiovascular and cerebrovascular diseases. Its therapeutic effects are often attributed to multi-target actions and generally favorable safety profiles. Ginkgo biloba leaves, a classical medicinal herb, contain bioactive compounds capable of modulating the onset and progression of ischemic stroke through multiple mechanisms [14–16].

Among these, diterpene lactones are the main pharmacologically active constituents, with Ginkgolide B (GB) being the most representative and demonstrating significant pharmacological activity [17]. Previous research has shown that GB exerts neuroprotective effects, improves endothelial function, and possesses anti-inflammatory and antioxidant activities [18–21], and exerts therapeutic effects in various free radical–related diseases, including IS [22,23], ischemic heart disease [24], chronic inflammation [25], and aging [26].

The AKT Serine/Threonine Kinase 1 (AKT1) signaling pathway, also referred to as the PI3K/AKT pathway, regulates a range of cellular processes, including survival, proliferation, metabolism, angiogenesis, migration, and apoptosis [27–30]. Evidence indicates that AKT1 is central to the pathophysiology of cardiovascular and cerebrovascular disorders, such as ischemic stroke [31], atherosclerosis [32], and hypertension [33]. Despite its established roles, it remains unclear whether GB can promote post-stroke angiogenesis by modulating AKT1 signaling, and this question has not been systematically addressed.

Building on these findings, this study aims to clarify how GB modulates the AKT1 signaling pathway to promote post-stroke angiogenesis. By elucidating these mechanisms, we hope to provide new insights into cerebrovascular repair and to identify therapeutic targets that may inform future treatment strategies.

2. Materials and Methods

2.1 Cell Line

The mouse brain microvascular endothelial cell line (bEnd.3, lot number CL-0598) was obtained from Wuhan Punosai Life Science Co., Ltd. Cells were maintained in high-glucose Dulbecco's Modified Eagle Medium (DMEM) supplemented with 5% fetal bovine serum (FBS) and 1% penicillin–streptomycin at 37 °C in a humidified incubator containing 5% CO_2, and were subcultured upon reaching 80–90% confluence. All cell lines were validated by STR profiling and tested negative for mycoplasma.

2.2 Drugs and Reagents

2.2.1 Chemicals

Ginkgolide B (GB; purity 98% by HPLC) was provided by the U.S. National Institute for Control of Pharmaceutical and Biological Products (Beijing, China). The powder was dissolved in dimethyl sulfoxide (DMSO; D2650) to prepare a 100 µM stock solution, which was stored at –20 °C protected from light and freshly prepared prior to use.

Based on the study by Zhou *et al.* [34], 3-n-Butylphthalide (NBP) was used as a positive control. NBP (≥98% purity, standard/powder) was purchased from MCE (Princeton, NJ, USA). The compound was dissolved in dimethyl sulfoxide (DMSO; D2650) to prepare a 100 µM stock solution, and working solutions at the desired concentrations were freshly prepared immediately before each experiment.

2.2.2 Reagents

Puromycin (lot number P8230) was purchased from Beijing Soleibao Biotechnology Co., Ltd. (Beijing, China). Fetal bovine serum (FBS; lot 164210-50), penicillin–streptomycin solution (lot PB180120), 0.25% trypsin–Ethylenediaminetetraacetic Acid (EDTA) (lot PB180229), high-glucose DMEM (lot PM150210), glucose-free DMEM (lot PM150270), PBS buffer (lot PB180327), and serum-free cryopreservation solution (lot PB180438) were all purchased from Wuhan Procell Co., Ltd. (Wuhan, China). Matrigel matrix (lot 356234) was purchased from BD Biosciences, (San Jose, CA, USA), and Transwell 24-well plates (lot 3422) were purchased from Corning (Corning, NY, USA). Bicinchoninic Acid (BCA) protein assay kit (catalog E-BC-K318-M) and Cell Counting Kit-8 (CCK-8) (catalog E-CK-A362) were purchased from Wuhan Elairuite Biotechnology Co., Ltd. (Wuhan, China). β-Actin antibody (catalog 20536-1-AP), Vascular Endothelial Growth Factor (VEGF) antibody (catalog 19003-1-AP), Angiogenin (ANG) antibody (catalog 18302-1-AP), Horseradish Peroxidase (HRP)-conjugated goat anti-rabbit Immunoglobulin G(IgG) (catalog SA00001-2) were purchased from Wuhan Proteintech Co., Ltd. (Wuhan, China). AKT1 antibody (catalog SAB4500796) was purchased from Merck KGaA (Darmstadt, Germany), Germany. AKT inhibitor MK2206 (catalog SF2712-10 mM) and 5-ethynyl-2′-deoxyuridine (EdU-488) cell proliferation detection kit (catalog C0071S) were purchased from Biyuntian Biotechnology Co., Ltd (Beijing, China). Radio-Immunoprecipitation Assay buffer (RIPA) protein lysis buffer (catalog CW2333s) was purchased from Kangwei Century Biotechnology Co., Ltd. (Beijing, China), and protease inhibitor (catalog A1320914) was purchased from AmBeed(Chicago, USA). Protein-free rapid blocking solution (catalog PS108P) and Omni-Flash™ ice-free rapid transfer buffer (catalog PS201S) were purchased from Shanghai Yamei Biopharmaceutical Technology Co., Ltd. (Shanghai, China). Enhanced chemiluminescence (ECL) reagent (catalog BL520B) was purchased from Biosharp (Beijing, China), and tissue fixative solution (catalog G1101) was purchased from Servicebio (Wuhan, China).

2.3 Instruments and Consumables

The following instruments were used in this study: incubator (model 3427), tri-gas incubator (model 3131), ultra-low temperature freezer (900 Series), and refrigerated high-speed centrifuge Fresco17 (Thermo Fisher Scientific, Waltham, MA, USA); low-speed centrifuge (Changsha Yingtai Instrument Co., Ltd. Changsha, China, model TD5A); constant-temperature water bath (Crystal Instruments, Silicon Valley, CA, USA, model SYG-1210); in-

verted microscope (ZEISS, Oberkochen, Germany, model AxioVert.A1); laminar flow cabinet (Suzhou Antai Air Technology Co., Ltd., Sujing Group, Suzhou, China, model SW-CJ-1F); multifunctional microplate reader (BioTek, VT, USA, model Cytation3); 0.22 µm Polyvinylidene Fluoride (PVDF) membrane (Millipore, MA, USA, catalog ISEQ00010); analytical microbalance (SHIMADZU, Kyoto, Japan, model AUW220D); power supply for general electrophoresis (Shanghai Yamei Biotechnology Co., Ltd., Shanghai, China, model UPS-600); and vertical electrophoresis chamber and transfer module (Bio-Rad, Hercules, USA, models Mini-PROTEAN® TetraCell and Mini Trans-Blot Module).

2.4 Potential Molecular Targets of GB in IS

2.4.1 Computational Prediction of GB Targets

The chemical structure of GB was retrieved from the PubChem database (https://pubchem.ncbi.nlm.nih.gov/) using the keyword "Ginkgolide B", and both its SMILES or 3D structure were downloaded (Fig. 1a). Potential targets of GB were obtained from the PharmMapper (http://www.lilab-ecust.cn/pharmmapper/) and TargetNet (http://targetnet.scbdd.com/) databases. After removing duplicates, all targets were mapped to their corresponding gene names using the UniProt database (https://www.uniprot.org/).

2.4.2 Acquisition of Angiogenesis- and Stroke-Related Genes

Genes related to angiogenesis were retrieved from the human GeneCards database (https://www.genecards.org) using the keyword "angiogenesis". Similarly, genes associated with stroke were obtained by querying the keyword "stroke" in the same database.

2.4.3 Identification of GB Intervention Targets

Data from Sections 2.4.1 and 2.4.2 were first combined. R software (R Foundation for Statistical Computing, Vienna, Austria) was then used to identify unique and overlapping targets among the groups. The results were visualized using the ggplot2 and VennDiagram packages to highlight potential GB targets involved in post-stroke angiogenesis.

2.5 Network Pharmacology Analysis

2.5.1 Protein–Protein Interaction (PPI) Network Construction

Protein–protein interaction (PPI) analysis of GB-related targets was conducted using the STRING database (https://cn.string-db.org/). The resulting network was visualized in Cytoscape software (Cytoscape Consortium, San Diego, CA, USA) to facilitate further analysis.

2.5.2 GO and KEGG Pathway Analysis

Gene Ontology (GO) and Kyoto Encyclopedia of Genes and Genomes (KEGG) enrichment analyses of GB-related targets were conducted using the ggplot2 package in R. Biological processes (BP), cellular components (CC), molecular functions (MF), and KEGG pathways were analyzed to explore the potential mechanisms by which GB may exert its effects in cerebral infarction.

2.5.3 Molecular Docking and Molecular Dynamics Simulation

Molecular docking and molecular dynamics (MD) simulations were performed to assess the interactions between GB and key angiogenesis-related proteins. Docking was carried out on the CB-Dock2 platform [35,36], which detects potential binding pockets using the CurPocket algorithm [37] and evaluates binding affinities with the AutoDock Vina scoring function. The crystal structures of AKT1 (PDB ID: 3O96), ANG (PDB ID: 1ANG), and VEGF (PDB ID: 4DEQ) were retrieved from the Protein Data Bank. GB was converted to mol2 format and docked into the five top-ranked binding pockets, and the conformation with the lowest binding energy was selected for further analysis. The resulting complexes were visualized in Discovery Studio 2021(BIOVIA, San Diego, CA, USA) and PyMOL v2.6 (Schrödinger, LLC, New York, NY, USA).

MD simulations were carried out using GROMACS v2022.03 (GROMACS Development Team) [38, 39]. The protein structures were parameterized with the AMBER99SB-ILDN force field, and ligand topologies were generated using the Generalized Amber Force Field (GAFF). Partial atomic charges were assigned via the restrained electrostatic potential (RESP) method implemented in Gaussian 16W. Each protein–ligand complex was solvated in a cubic Transferable Intermolecular Potential with 3 Points (TIP3P) water box, keeping at least 1.2 nm between the solute and the box edge, and counterions (Na^+) were added to neutralize the system. Energy minimization was performed using the steepest descent algorithm. Short-range electrostatic and van der Waals cutoffs were set to 1.0 nm, and long-range electrostatics were treated with the particle mesh Ewald (PME) method. All bonds involving hydrogen atoms were constrained using the LINCS algorithm. The system was equilibrated under constant number of particles, volume, and temperature (NVT) and constant number of particles, pressure, and temperature (NPT) ensembles for 100 ps each to stabilize temperature and pressure. Subsequently, a 50 ns production run was performed under NPT conditions at 300 K and 1 bar, using a 2 fs integration step. Trajectories were recorded every 10 ps for further analysis.

Following the simulations, we analyzed the trajectories to examine the structural stability and binding dynamics of the protein–ligand complexes. The root-mean-square deviation (RMSD), radius of gyration (Rg), root-

mean-square fluctuation (RMSF), solvent-accessible surface area (SASA), and hydrogen bond number were calculated to assess conformational stability and overall compactness. To further characterize the energetic landscape, Gibbs free energy surfaces were constructed using the g_sham module in GROMACS. Binding free energies were then estimated with the MM/PBSA approach implemented in gmx_MMPBSA, using snapshots extracted from the final 20 ns of the production trajectories.

2.6 Experimental Validation

2.6.1 Establishment of the Oxygen–Glucose Deprivation/Reperfusion (OGD/R) Model

To induce oxygen–glucose deprivation (OGD), the culture medium was replaced with glucose-free DMEM, and bEnd.3 cells were incubated under hypoxic conditions (1% O_2, 5% CO_2, 94% N_2) at 37 °C for 6 hours. After hypoxic exposure, the medium was changed to complete DMEM, and the cells were returned to normoxic conditions for 24 hours to allow reperfusion.

2.6.2 Experimental Grouping and Drug Administration

The study included six experimental groups: control, model, 10 μM GB, 20 μM GB, 40 μM GB, and NBP. The control group was maintained under normoxic conditions, whereas the model group was subjected to OGD/R as described above. For GB treatment, cells underwent OGD for 6 hours and were then incubated with GB at final concentrations of 10, 20, or 40 μM during the 24-hour reperfusion period. The positive control group received 10 μM NBP under the same post-OGD/R conditions.

2.6.3 CCK-8 Assay

To determine the safe concentration range of GB, bEnd.3 cells were cultured in a control group (0 μM) and treatment groups with varying GB concentrations (0, 5, 10, 20, 40, 80, and 160 μM). After 24 hours, cell viability was measured using the CCK-8 assay. Briefly, 10 μL of CCK-8 reagent was added to each well containing 100 μL of fresh medium, and the plates were incubated at 37 °C with 5% CO_2 for 2 hours. Absorbance at 450 nm was recorded using a multifunctional microplate reader to identify the optimal GB concentration for subsequent experiments.

2.6.4 EdU Assay

After OGD/R treatment, bEnd.3 and control cells were seeded at 1.8×10^4 cells per well in 24-well plates and incubated overnight to allow adhesion. The medium was then refreshed, and cells were maintained under normoxic conditions for 24 hours. Cells were subsequently incubated with 10 μM EdU for 4 hours. After EdU exposure, the medium was removed, and cells were fixed with 4% paraformaldehyde for 15 minutes, washed with PBS, and permeabilized with 0.3% Triton X-100, followed by another PBS wash. The Click reaction solution was prepared according to the kit instructions (per well: 86 μL Click Reaction Buffer, 4 μL $CuSO_4$, 0.2 μL Azide488, and 10 μL Click Additive Solution) and 100 μL was added to each well. Plates were incubated in the dark for 30 minutes and washed with PBS. Nuclei were counterstained with 1× Hoechst 33342 (1:1000 in PBS) at room temperature in the dark for 10 minutes, washed, and imaged using fluorescence microscopy. EdU-positive cells emitted green fluorescence (Alexa Fluor 488), while nuclei appeared blue.

2.6.5 Wound Healing Assay

To standardize imaging positions across samples, five evenly spaced horizontal reference lines were drawn on the underside of each 6-well plate. bEnd.3 cells were seeded at a density of 2×10^5 cells per well and grown to approximately 85% confluence. To synchronize the cell cycle, cultures were serum-deprived for 24 hours before scratching. A uniform linear wound was then generated using a sterile pipette tip, and floating cells were removed by two gentle PBS washes. Images of the same regions were captured at 0 and 24 hours under a phase-contrast microscope, and the wound closure percentage was calculated accordingly. The wound closure rate was quantified using the following equation:

$$\text{Wound closure (\%)} = \frac{w_0 - w_t}{w_0} \times 100$$

Where W_0 represents the initial wound width and W_t denotes the wound width measured after 24 hours.

2.6.6 Transwell Assay

For the Transwell migration assay, cells were harvested by trypsinization, resuspended in serum-free medium, and adjusted to a density of 1.8×10^5 cells/mL. An aliquot of 110 μL ($\approx 2 \times 10^4$ cells) was added to the upper chamber of each insert. Both the upper and lower chambers initially contained glucose-free DMEM to mimic ischemic conditions. After 6 hours of OGD/R exposure, 500 μL of complete medium (high-glucose DMEM supplemented with 10% FBS and 1% penicillin-streptomycin) was placed in the lower chamber to establish a chemotactic gradient. The plates were incubated for 24 hours at 37 °C in a humidified atmosphere of 5% CO_2 and 95% air. Non-migrated cells remaining on the upper membrane surface were removed gently with a cotton swab. The inserts were fixed in 4% paraformaldehyde for 30 minutes, stained with 0.1% crystal violet for 30 minutes, rinsed thoroughly with PBS, and air-dried. Migrated cells were imaged in five random microscopic fields and quantified using ImageJ software (National Institutes of Health, Bethesda, MD, USA); the mean cell number was normalized to the control group.

2.6.7 Tube Formation Assay

For the tube formation assay, growth factor–reduced Matrigel was thawed on ice, aliquoted at 50 μL per well, and allowed to solidify at 37 °C for 30 minutes. bEnd.3 cells were harvested by trypsinization, resuspended in serum-

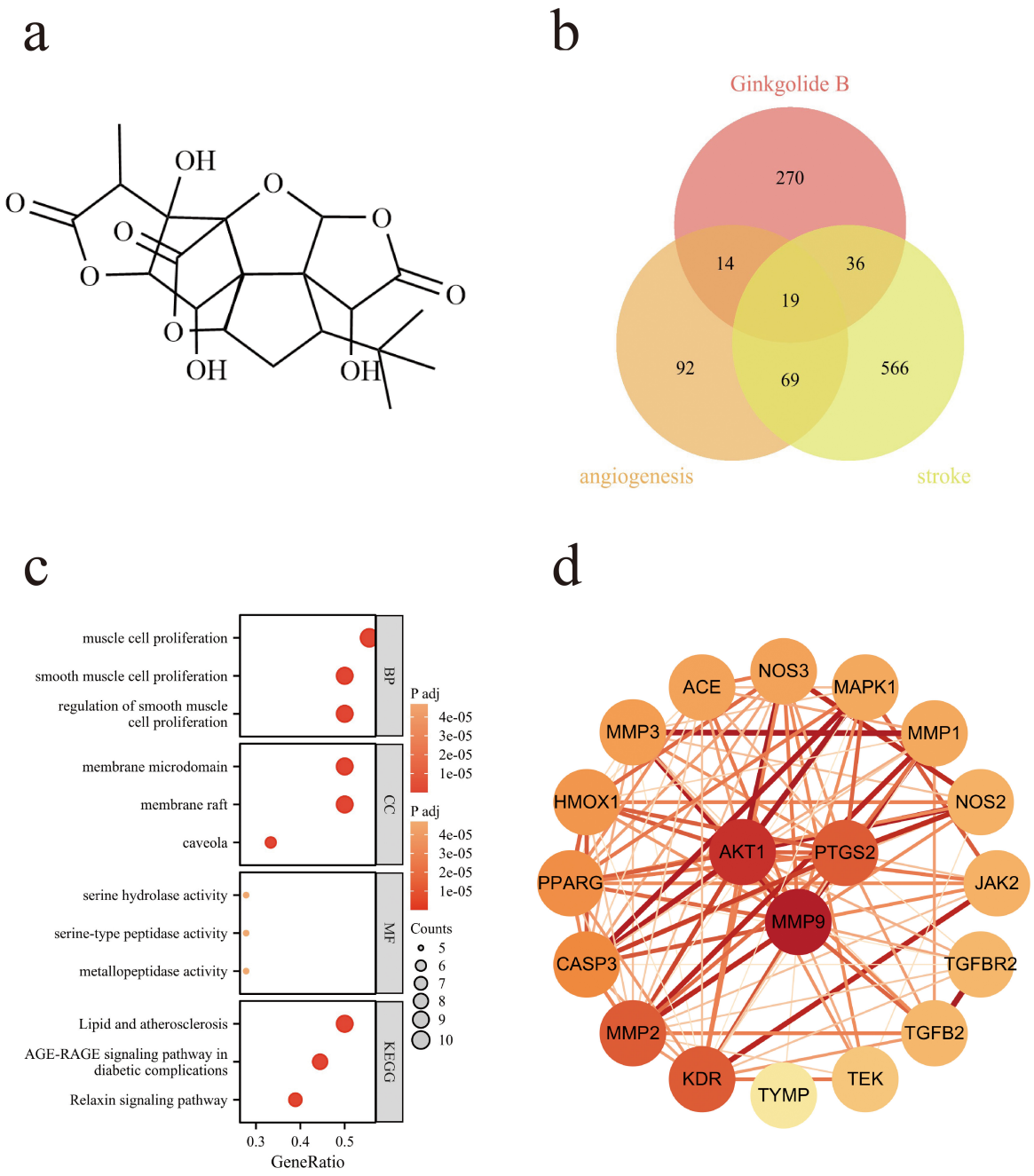

Fig. 1. Network pharmacology analysis of GB targets. (a) Chemical structure of GB. (b) Venn diagram showing the overlap among predicted GB targets, ischemic stroke-related genes, and angiogenesis-related genes. (c) GO and KEGG enrichment analyses of the overlapping targets. (d) PPI network of the 19 overlapping targets. GB, Ginkgolide B; PPI, Protein–protein interaction.

free medium, and adjusted to a final concentration of 1.8×10^5 cells/mL. A 100 µL suspension ($\approx 1.8 \times 10^4$ cells) was carefully seeded onto the polymerized Matrigel and subjected to the indicated experimental treatments. After approximately 6 hours of incubation, capillary-like structures were imaged under an inverted microscope. Tube formation was quantified by counting branch points and measuring total tube length in five randomly selected microscopic fields per well using ImageJ software, and the data were normalized to the control group.

2.6.8 Western Blot Analysis

Total protein was extracted from each experimental group using RIPA buffer supplemented with protease inhibitors. Protein concentrations were determined with a BCA assay kit, and equal amounts of protein were resolved by SDS–PAGE at 160 V for 45 minutes. Proteins were subsequently transferred onto PVDF membranes at a constant current of 300 mA for 30 minutes. Membranes were blocked with a rapid protein-free blocking buffer and incubated overnight at 4 °C with the following primary an-

tibodies: AKT1 (1:1000), VEGF (1:5000), Ang (1:1000), and β-actin (1:8000). After thorough washing, membranes were incubated with HRP-conjugated goat anti-rabbit IgG secondary antibodies (1:10,000) for 1 hour at room temperature. Protein bands were detected using enhanced chemiluminescence reagents and imaged with a ChemiDoc system. Densitometric analysis was performed with Image Lab software, and band intensities were normalized to β-actin.

2.7 Statistical Analysis

Statistical analyses were conducted using SPSS version 26.0 (IBM Corp., Armonk, NY, USA). Data are expressed as mean $\pm$ standard deviation (mean $\pm$ SD). For comparisons among multiple groups, one-way analysis of variance (ANOVA) was applied when the assumptions of normality and homogeneity of variance were met, followed by Least Significant Difference (LSD) or Tukey post hoc tests for pairwise comparisons. If variances were unequal, the Games-Howell test was employed, whereas non-normally distributed data were analyzed using the Kruskal-Wallis rank-sum test. A p-value < 0.05 was considered statistically significant. Graphs were prepared in GraphPad Prism version 10.0 (GraphPad Software, San Diego, CA, USA), with image analyses conducted in ImageJ and additional figures generated in R.

3. Results

3.1 Identification of Potential Molecular Targets of GB in IS

Potential targets of GB were initially identified using PharmMapper and TargetNet, yielding 299 and 58 candidates, respectively. Representative targets from PharmMapper included NR1H2, GSTP1, BCHE, METAP1, and GBA, while TargetNet examples comprised NOS2, CHRM4, CASP9, NR2F2, and NR3C1. All targets were mapped to gene symbols via the UniProt database, though eight proteins lacked annotations. After removing duplicates, a total of 339 unique GB targets were retained. Genes associated with angiogenesis and stroke were retrieved from GeneCards (https://www.genecards.org) using a relevance score threshold of $\geq$2, resulting in 194 angiogenesis-related and 690 stroke-related genes. Overlapping and unique genes were analyzed in R and visualized with the ggplot2 and VennDiagram packages (Fig. 1b), ultimately identifying 19 putative GB targets.

3.2 Network Pharmacology Analysis

The PPI analysis of the 19 predicted GB targets identified 110 interaction pairs, with AKT1, MMP9, and PTGS2 exhibiting the highest connectivity (Fig. 1d). GO and KEGG enrichment analyses were performed with a significance threshold of $p < 0.05$, revealing that these targets are primarily involved in inflammation, oxidative stress, apoptosis, and angiogenesis (Fig. 1c). Key enriched signaling pathways included PI3K–Akt, MAPK, HIF-1, VEGF, and TNF/NF-κB. Collectively, these findings suggest that GB may exert protective effects in ischemic stroke by modulating inflammatory and apoptotic processes, mitigating oxidative stress and metabolic dysfunction, and promoting angiogenesis through multiple interconnected pathways.

3.3 Molecular Docking and Molecular Dynamics Simulation

To evaluate the potential of GB in regulating angiogenesis, molecular docking and molecular dynamics simulations were performed to systematically assess its interactions with key angiogenesis-related proteins. Docking analysis revealed that GB binds to AKT1 with a binding energy of –10.2 kcal/mol, forming hydrogen bonds with Glutamine (GLN79), Asparagine (ASN54), and Tyrosine (TYR326), a carbon–hydrogen bond with TYR272, and a repulsive interaction with ARG273 (Fig. 2a). Comparable intermolecular interaction patterns were also observed with ANG and VEGF (Fig. 2b,c).

MD simulations were performed to assess the stability and conformational dynamics of GB bound to AKT1, ANG, and VEGF (Fig. 3). RMSD analysis (Fig. 3a) indicated that the AKT1–GB and ANG–GB complexes remained below 0.35 nm, reflecting structural stability, whereas the VEGF–GB complex exhibited larger fluctuations (>1 nm), indicative of conformational instability. Ligand RMSD (Fig. 3b) confirmed greater mobility of GB within the VEGF complex, consistent with weaker binding. Radius of gyration (Rg) analysis (Fig. 3c) showed that AKT1 and ANG maintained extended, stable conformations (Rg $\approx$ 2.0–2.5 nm), whereas VEGF adopted a more compact structure (Rg $\approx$ 1.5 nm).

Solvent-accessible surface area (SASA) analysis (Fig. 3d) supported these observations, with AKT1 exhibiting the largest accessible surface (~220 nm^2), ANG the smallest (~90 nm^2), and VEGF intermediate (~120 nm^2). RMSF analysis (Fig. 3e) revealed localized flexibility, with AKT1 residues 100–150 showing minor fluctuations (RMSF <0.5 nm), ANG remaining largely rigid, and VEGF displaying pronounced fluctuations around residue 200 (>1 nm). Hydrogen bond analysis (Fig. 3f) indicated that the ANG–GB complex formed the greatest number of hydrogen bonds (2–10), followed by AKT1 (2–5), while VEGF formed the fewest, consistent with weaker interactions.

Gibbs free energy landscape analysis (Fig. 3g) demonstrated that the ANG–GB complex occupied the deepest energy basin, reflecting the most stable conformation. AKT1 adopted moderately flexible but stable states, whereas VEGF exhibited a scattered energy distribution with multiple metastable states. Molecular mechanics/Poisson–Boltzmann surface area (MM/PBSA) calculations (Fig. 3h) revealed that GB had the strongest binding affinity for AKT1 (ΔG_bind = –39.87 kcal/mol), with weaker interactions observed for ANG (–18.90 kcal/mol) and VEGF

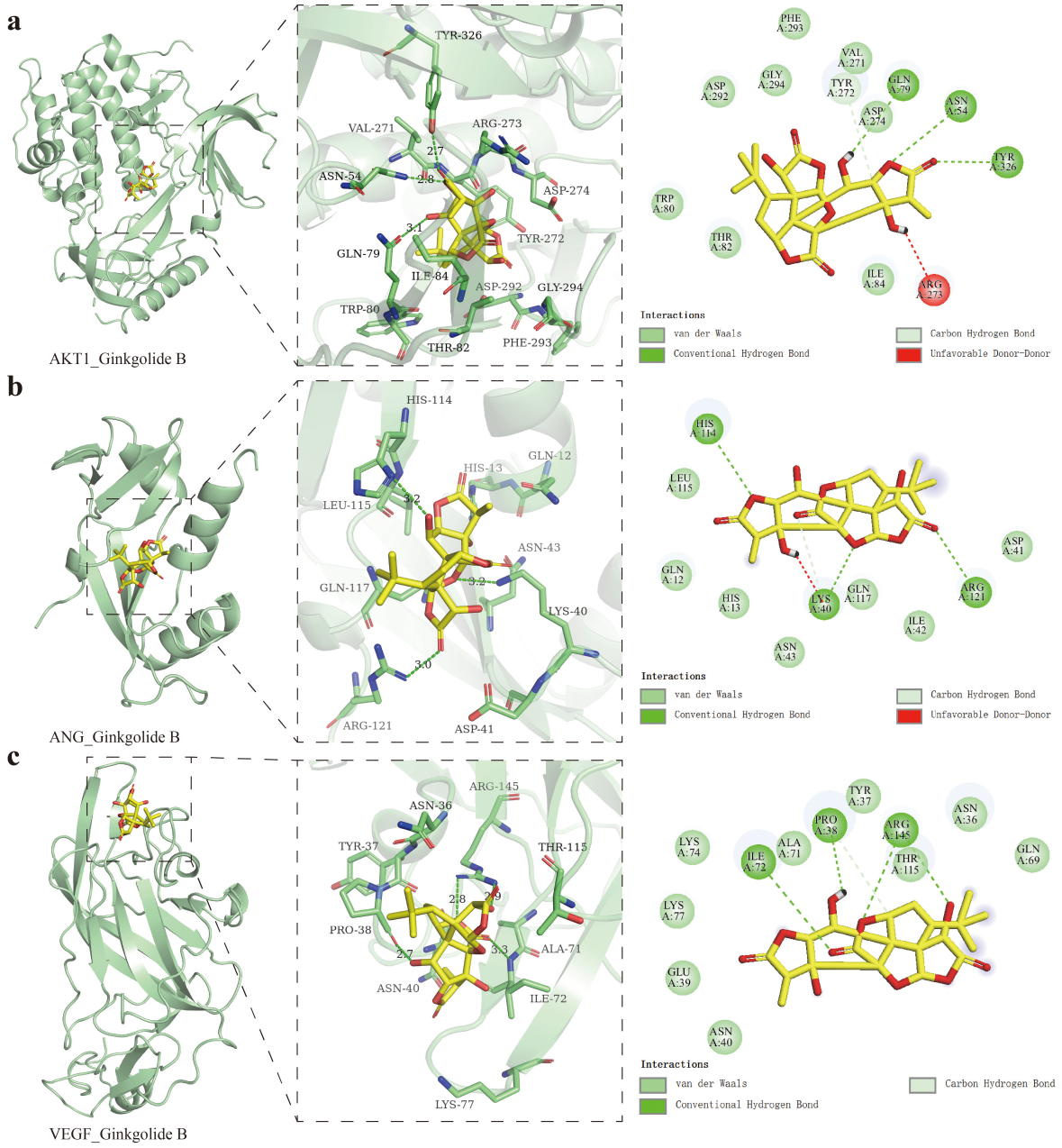

Fig. 2. Molecular docking results. (a) Molecular docking of GB with AKT1. (b) Molecular docking of GB with ANG. (c) Molecular docking of GB with VEGF.

(–22.02 kcal/mol). Collectively, these results suggest that GB forms the most stable complex with ANG and AKT1, whereas its interaction with VEGF is comparatively weaker, consistent across multiple stability and energy metrics.

3.4 Effect of GB on Viability of bEnd.3 Cells Under OGD/R-Induced Injury

The safe concentration range of GB was determined using the CCK-8 assay. In normal bEnd.3 cells, treatment with GB at 5, 10, 20, and 40 μM had no significant effect on cell viability, whereas higher concentrations (80 and 160 μM) caused marked cytotoxicity (Fig. 4a,b). In the OGD/R model, cell viability was significantly reduced; treatment with GB at 10, 20, or 40 μM effectively attenuated this injury in a dose-dependent manner. Based on these results, 10, 20, and 40 μM were selected for subsequent experiments to investigate the stress-repair effects of GB and its underlying mechanisms in OGD/R-induced bEnd.3 cell injury.

3.5 Effect of GB on bEnd.3 Cell Proliferation in an OGD/R-Induced Injury Model

To evaluate the effect of GB on endothelial cell proliferation, EdU assays were performed in bEnd.3 cells. Results showed that treatment with GB at 20, and 40 μM, as

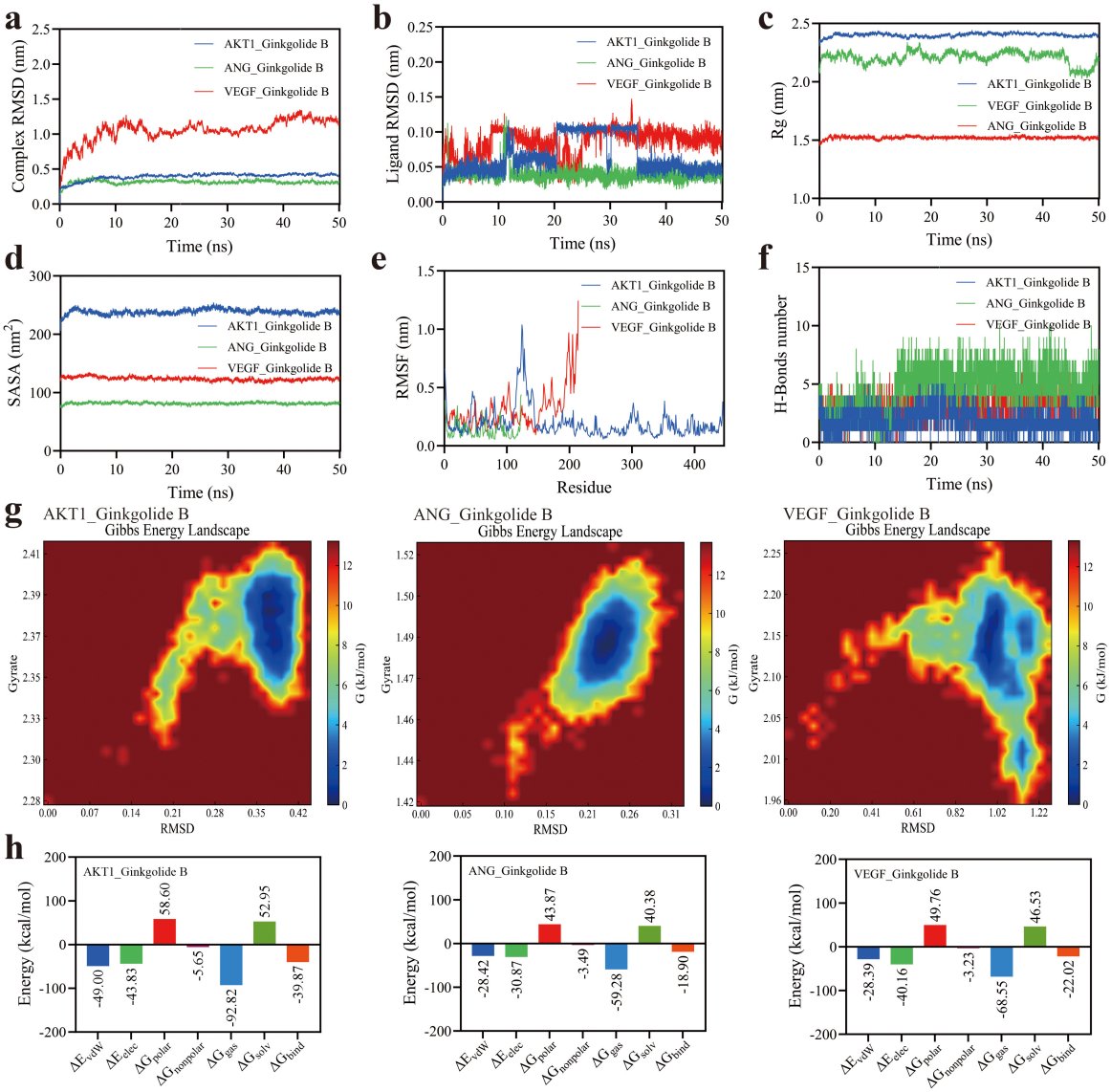

Fig. 3. MD simulation analysis of the GB–protein complexes over 50 ns. (a) RMSD of the complexes. (b) RMSD of GB ligands. (c) Rg of proteins. (d) SASA of proteins. (e) RMSF of proteins. (f) Number of hydrogen bonds between GB and proteins. (g) Gibbs free energy landscape of the complexes. (h) Binding free energy of GB–protein interactions calculated by MM/PBSA. RMSD, root-mean-square deviation; Rg, radius of gyration; SASA, solvent-accessible surface area; RMSF, root-mean-square fluctuation.

well as with NBP, for 24 h significantly increased the proportion of EdU-positive cells relative to the control ($p < 0.01$; Fig. 4c,e). The proliferative effect of 40 μM GB was comparable to that of NBP, suggesting that this concentration effectively promotes bEnd.3 cell proliferation, consistent with observations from the CCK-8 assay.

Significant differences in endothelial cell proliferation were observed among the treatment groups (Fig. 5a,d). OGD/R treatment alone increased the proportion of EdU-positive cells relative to the control ($p < 0.01$), and GB treatment further enhanced proliferation under these conditions ($p < 0.01$). In contrast, the AKT1 inhibitor MK2206 markedly suppressed proliferation ($p < 0.01$). Co-treatment with GB and MK2206 partially rescued proliferation compared with the MK2206-only group, although it remained lower than GB treatment alone ($p < 0.01$). These findings suggest that GB promotes endothelial cell proliferation under OGD/R stress, at least in part through activation of the AKT1 signaling pathway.

3.6 GB and the Migratory Capacity of bEnd.3 Cells Under OGD/R-Induced Injury

The migratory capacity of bEnd.3 cells was evaluated using wound healing and Transwell assays (Fig. 4d,f,g,i). OGD/R treatment significantly increased cell migration relative to the control ($p < 0.01$), indicating enhanced migratory activity following injury. GB treatment at 20 and 40 μM, as well as NBP, further promoted migration ($p < 0.01$),

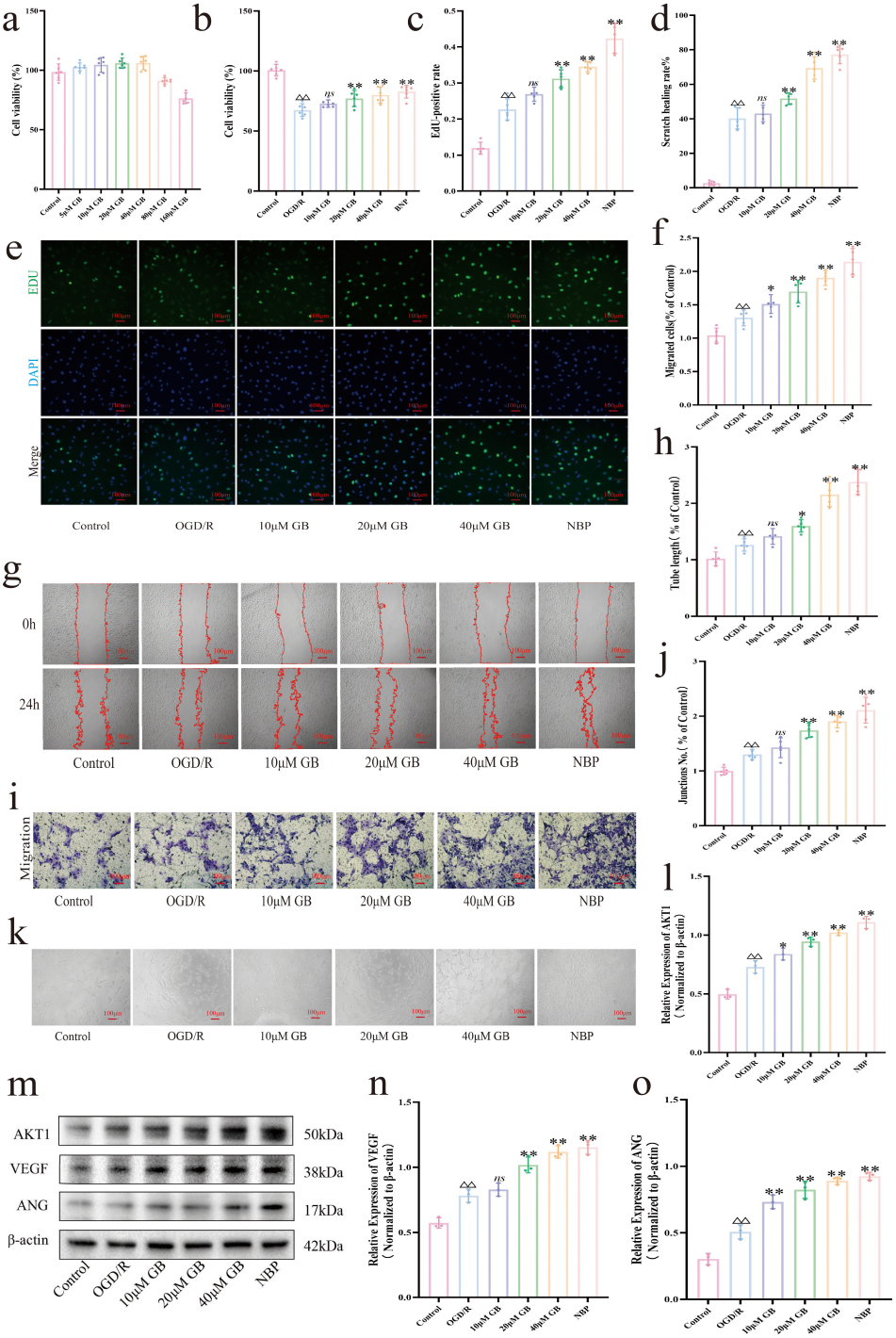

Fig. 4. GB promotes angiogenesis *in vitro*. (a) CCK-8 assay evaluating the effects of different concentrations of GB on bEnd.3 cell viability (n = 6). (b) CCK-8 assay assessing bEnd.3 cell viability following GB intervention at different concentrations (n = 6). (c) Quantification of EdU-positive cells after GB treatment (n = 5). (d) Quantitative analysis of horizontal migration of bEnd.3 cells (n = 5). (e) Representative EdU intake assay (Scale bar, 100 μm, 100×). (f) Quantitative analysis of vertical migration of bEnd.3 cells (cells passing through Matrigel-free Transwell chambers, n = 5). (g) Representative images of wound healing assay in bEnd.3 monolayers (Scale bar, 100 μm, 100×). (h) Quantification of the tube length (n = 5). (i) Representative images of invasive bEnd.3 cells (Scale bar, 100 μm, 100×). (j) Quantification of branch points (n = 5). (k) Representative images of tube formation by bEnd.3 cells (Scale bar, 100 μm, 100×). (m) Representative Western blot images of AKT1, VEGF, and ANG. (l,n,o) Expression levels of angiogenesis-related proteins AKT1, VEGF, and ANG in each group (n = 3). Data are presented as mean ± SD. $\triangle\triangle p < 0.01$ vs. control group; $*p < 0.05$, $**p < 0.01$ vs. OGD/R group; ns, not significant. CCK-8, Cell Counting Kit-8; EdU, 5-ethynyl-2′-deoxyuridine; AKT1, AKT Serine/Threonine Kinase 1; VEGF, Vascular Endothelial Growth Factor; ANG, Angiogenin; OGD/R, oxygen–glucose deprivation/reperfusion.

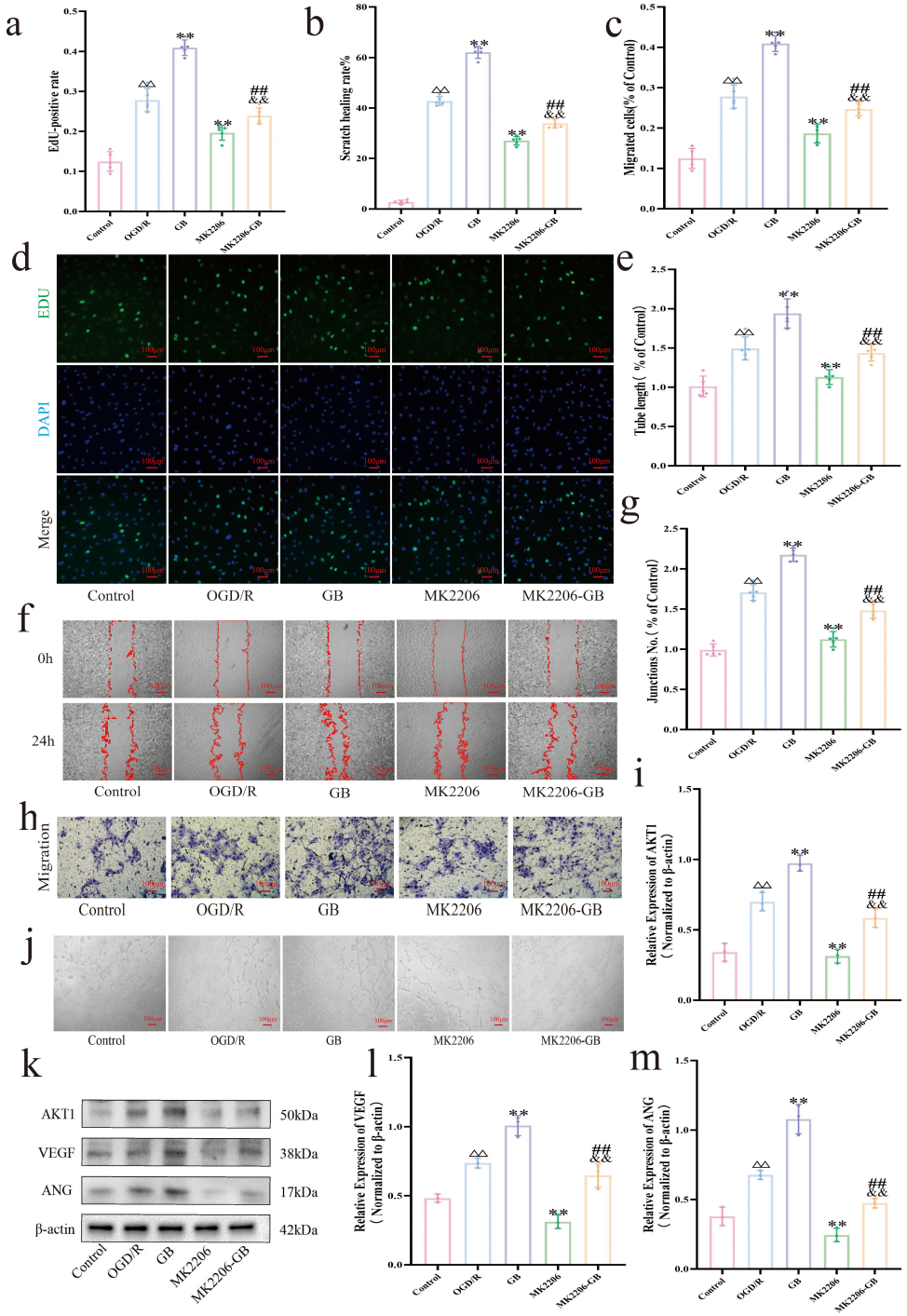

Fig. 5. Ginkgolide B promotes angiogenesis and exerts neuroprotective effects through activation of the AKT1/VEGF/Ang signaling pathway. (a) Quantification of EdU-positive cells (n = 5). (b) Quantitative analysis of horizontal migration of bEnd.3 cells (n = 5). (c) Quantitative analysis of vertical migration of bEnd.3 cells (cells passing through Matrigel-free Transwell chambers, n = 5). (d) Representative EdU intake assay (Scale bar, 100 μm, 100×). (e) Quantification of the tube length (n = 5). (f) Representative images of wound healing assay in bEnd.3 monolayers (Scale bar, 100 μm,100×). (g) Quantification of branch points (n = 5). (h) Representative images of invasive bEnd.3 cells (Scale bar, 100 μm,100×). (j) Representative images of tube formation by bEnd.3 cells (Scale bar, 100 μm, 100×). (k) Representative Western blot images of AKT1, VEGF, and ANG. (i,l,m) Expression levels of angiogenesis-related proteins AKT1, VEGF, and ANG in each group (n = 3). Data are presented as mean ± SD. $\triangle\triangle p < 0.01$ vs. control group; $^{**}p < 0.01$ vs. OGD/R group; $\#\#p < 0.01$ vs. GB group; $\&\&p < 0.01$ vs. MK2206 group.

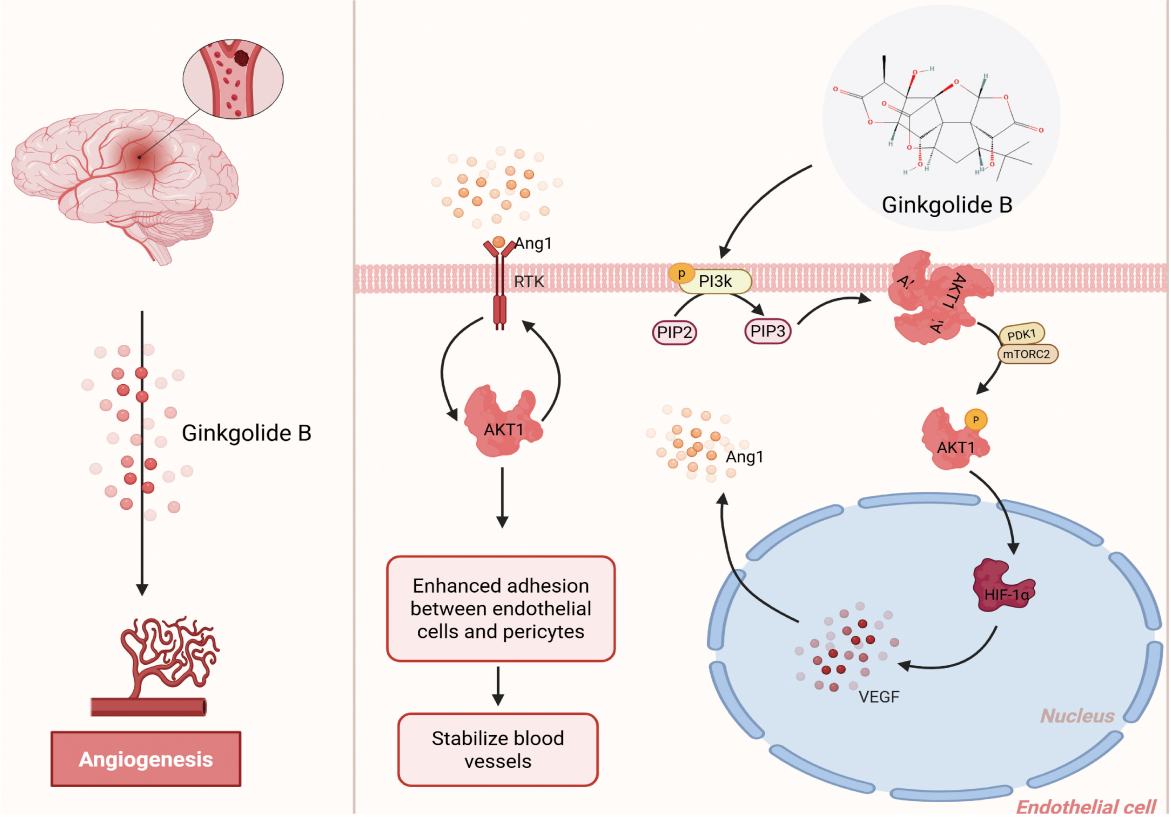

Fig. 6. Schematic representation of the angiogenic mechanism of GB following ischemic brain injury. GB activates the PI3K/AKT signaling pathway in endothelial cells, which subsequently promotes HIF-1α–dependent VEGF expression and facilitates Ang1-mediated interactions between endothelial cells and pericytes. These processes stabilize vascular structures, enhance angiogenesis, and improve blood perfusion in ischemic brain tissue. (Created with BioRender.com.)

with 40 µM GB producing the most pronounced effect. In contrast, 10 µM GB caused only a modest, non-significant increase, suggesting that lower concentrations may be insufficient to fully activate AKT1 signaling and stimulate migration.

Migration analysis across treatment groups (Fig. 5b,c,f,h) showed that OGD/R significantly enhanced cell migration compared with the control ($p < 0.01$). GB treatment further promoted migration under OGD/R conditions ($p < 0.01$). The AKT1 inhibitor MK2206 markedly suppressed migration ($p < 0.01$), highlighting the critical role of AKT1. Co-treatment with GB and MK2206 partially rescued migration relative to the MK2206-only group, although the effect remained lower than with GB alone ($p < 0.01$).

3.7 Effect of GB on Tube Formation by bEnd.3 Cells Under OGD/R-Induced Injury

The effect of GB on angiogenic activity under OGD/R conditions was evaluated using a tube formation assay in bEnd.3 cells (Fig. 4h,j,k). OGD/R significantly increased both the number of branch points and the total branch length compared with the control ($p < 0.01$), indicating enhanced tube formation. Treatment with GB at 20 and 40 µM, as well as NBP, further promoted these angiogenic parameters ($p < 0.05$ or $p < 0.01$), with 40 µM GB producing the most pronounced effect.

Tube formation analysis across treatment groups (Fig. 5e,g,j) showed that OGD/R significantly increased both the number of branch points and total branch length compared with the control ($p < 0.01$), indicating enhanced tube-forming capacity of bEnd.3 cells. The AKT1 inhibitor MK2206 markedly reduced these parameters relative to the OGD/R group ($p < 0.01$), highlighting the critical role of AKT1 in tube formation. In GB-treated groups, branch points and total branch length were significantly increased ($p < 0.01$); however, co-treatment with MK2206 partially attenuated these effects ($p < 0.05$). These findings suggest that GB promotes tube formation after OGD/R injury, at least in part through AKT1 signaling.

3.8 Effect of Ginkgolide B on the Expression of Key Angiogenic Proteins in an OGD/R-Induced bEnd.3 Cell Injury Model

VEGF and Ang are key mediators of endothelial cell angiogenesis, and their expression is regulated by AKT1. Western blot analysis (Fig. 4l–o) showed that OGD/R significantly upregulated VEGF, Ang, and AKT1 protein lev-

els compared with the control ($p < 0.01$). GB treatment at 20 and 40 μM, as well as NBP, further enhanced the expression of these proteins ($p < 0.01$), consistent with a role in promoting angiogenic signaling.

Protein expression analysis across treatment groups (Fig. 5i,k–m) showed that OGD/R significantly upregulated VEGF, Ang, and AKT1 compared with the control ($p < 0.01$). OGD/R significantly upregulated VEGF, Ang, and AKT1 compared with the control ($p < 0.01$). GB treatment further increased the levels of these proteins ($p < 0.01$), whereas AKT1 inhibition markedly reduced them ($p < 0.01$). Co-treatment with GB in the presence of MK2206 partially restored VEGF, Ang, and AKT1 expression ($p < 0.01$). These findings suggest that GB promotes angiogenesis and exerts the stress-repair effects on endothelial cells, at least in part through activation of the AKT1–VEGF/Ang signaling axis.

4. Discussion

In this study, we combined network pharmacology with molecular simulations to investigate the potential mechanisms by which GB may promote angiogenesis following IS. Analysis of the PharmMapper and TargetNet databases identified 339 potential GB targets. Additionally, 194 angiogenesis-related genes and 690 stroke-related genes were retrieved from GeneCards, with intersection analysis yielding 19 candidate targets. PPI network analysis highlighted AKT1, MMP9, and PTGS2 as central nodes. GO and KEGG enrichment analyses revealed that these targets are primarily involved in inflammation, oxidative stress, apoptosis, and angiogenesis, with significant enrichment in PI3K–Akt, MAPK, HIF-1, VEGF, and TNF/NF-κB signaling pathways. Molecular docking and molecular dynamics simulations further indicated that AKT1 is the most favorable binding target of GB, exhibiting the strongest binding affinity.

In vitro, GB at safe concentrations ($\leq$40 μM) significantly attenuated OGD/R-induced endothelial injury, as evidenced by improved cell viability, enhanced proliferation and migration, and increased tube formation. The pro-angiogenic effect of 40 μM GB was comparable to that of the positive control NBP and consistent with the cytotoxicity assay results, suggesting that GB exerts both neuroprotective and vasculoprotective effects.

Previous studies have shown that AKT1 activation promotes angiogenesis in ischemic regions by regulating VEGF [40–42], thereby facilitating vascular reconstruction following cerebral infarction [43–45]. VEGF, a central angiogenic mediator, maintains vascular network stability after stroke by controlling the dynamic balance between tip and stalk cells [46]. While Ang supports endothelial cell survival, neovessel maturation, and vascular stabilization [47]. Under OGD/R conditions, the observed increase in angiogenic responses mediated by VEGF and ANG likely reflects a tissue stress response to ischemia, aimed at repairing vascular damage. However, excessive oxidative stress and inflammatory cascades following ischemia appear to limit the effectiveness of this endogenous response, such that elevated VEGF and ANG levels are insufficient to fully ameliorate extensive ischemic injury. Previous studies have demonstrated that neovascular formation exhibits pronounced spatiotemporal heterogeneity: early neovessels are often structurally immature, functionally compromised, and prone to leakage, potentially exacerbating tissue damage. Treatment with GB was associated with further increases in AKT1, VEGF, and ANG levels, suggesting that GB may potentiate angiogenic signaling beyond the capacity of intrinsic repair mechanisms. Accordingly, GB treatment appears to support the formation of stable capillaries, maintain endothelial cell function in nascent vessels, enhance local perfusion, and partially mitigate post-ischemic neurological deficits. To examine whether GB's pro-angiogenic effects depend on AKT1, we used the AKT1 inhibitor MK2206. MK2206 treatment partially reversed the OGD/R- and GB-induced increases in total AKT1 levels, significantly downregulated AKT1 expression, reduced VEGF and Ang levels, and suppressed endothelial cell proliferation, migration, and tube formation, indicating that AKT1 is a key regulator of angiogenesis under ischemic and hypoxic conditions. Conversely, GB treatment upregulated AKT1 and its downstream effectors, partially reversing the inhibitory effects of MK2206, confirming that GB promotes angiogenesis at least in part through AKT1 pathway activation.

The pathological process of ischemic brain injury is highly complex, involving excitotoxicity, inflammation, angiogenesis, and neurogenesis [48]. Increasing evidence suggests that GB exerts neuroprotective and pro-angiogenic effects through multiple targets and pathways. Wei and Tang [49] reported that GB inhibits platelet activation, reduces β-amyloid (Aβ)-induced neurotoxicity, and activates the PI3K/AKT pathway to promote neuronal regeneration. GB has also been shown to upregulate brain-derived neurotrophic factor (BDNF), enhancing neuronal survival, suppressing apoptosis, and facilitating neural repair [50], thereby contributing to neovascularization [51]. Shu *et al*. [52] demonstrated that GB attenuates post-stroke brain injury and improves neurological function by activating the platelet-activating factor (PAF) receptor, shifting microglia/macrophages from the pro-inflammatory M1 phenotype to the anti-inflammatory M2 phenotype. Additionally, Zhu *et al*. [53] reported that GB regulates the CCT/TRiC–SK1 axis by inhibiting creatine kinase B (CKB) activity, improving cerebral blood flow, promoting microvascular neogenesis, and protecting endothelial cells. GB also enhances antioxidant protein expression via the AKT/Nrf2 pathway, alleviating oxidative stress and promoting angiogenesis [54]. These studies collectively highlight the multifaceted role of GB in stroke therapy. Several Chinese patent medicines, such as Ginkgolide Meglumine

Dispersible Tablets, incorporate GB as a core component to mitigate neuronal injury after stroke; however, the precise mechanisms underlying its pro-angiogenic effects remain incompletely understood.

Although GB generally enhanced endothelial cell viability, proliferation, migration, and tube formation, variability was observed across experiments. At 10 μM, increases in migration, proliferation, and branch point formation were inconsistent and, in several cases, did not reach statistical significance. This variability appeared more pronounced under conditions of lower cell confluence or less stable OGD/R treatment, suggesting that experimental context influences GB's effects. Mild batch-to-batch fluctuations in VEGF and Ang expression were also noted, indicating that upstream signaling may vary with cellular state or culture conditions. Collectively, these findings suggest that GB's effects are not strictly dose-linear and may involve a threshold-dependent mechanism. Larger-scale and inter-laboratory studies will be important to further evaluate the robustness and reproducibility of these observations.

While this study systematically elucidated the mechanisms by which GB promotes angiogenesis via the AKT1/VEGF/Ang signaling pathway (Fig. 6), several limitations should be acknowledged. First, angiogenesis is a dynamic, time-dependent process, yet the present study did not fully characterize the dose–response relationship or temporal dynamics of GB's effects. Second, *in vitro* models cannot completely replicate the complex microenvironment of cerebral infarction or the dynamic regulation of the blood–brain barrier, and the pro-angiogenic and neuroprotective effects of GB were not validated *in vivo*. Third, this investigation focused primarily on a single signaling pathway, without examining other critical regulators such as Notch, HIF-1α, or Wnt/β-catenin. Future studies should employ animal models of cerebral infarction to validate *in vivo* effects and incorporate genomic or proteomic approaches to explore additional signaling pathways. Furthermore, co-culture systems or blood–brain barrier models could better simulate complex microenvironments, while gene-editing or pharmacological interventions may help dissect upstream regulatory mechanisms. These strategies would provide a more comprehensive evaluation of GB's safety, pharmacokinetics, and translational potential.

In conclusion, by combining network pharmacology, molecular simulations, and cellular experiments, this study elucidates the mechanisms by which GB promotes angiogenesis through the AKT1/VEGF/Ang signaling pathway. These results provide direct evidence for GB's role in vascular repair following ischemic stroke and lay a foundation for its further development and potential clinical translation.

Abbreviations

GB, Ginkgolide B; OGD/R, oxygen–glucose deprivation/reperfusion; PPI, protein–protein interaction; IS, Ischemic stroke; TCM, traditional Chinese medicine; AKT1, The AKT Serine/Threonine Kinase 1; FBS, fetal bovine serum; NBP, 3-n-Butylphthalide; VEGF, Vascular Endothelial Growth Factor; CCK-8, Cell Counting Kit-8; ANG, Angiogenin; BP, biological processes; CC, cellular components; MF, molecular functions; MD, molecular dynamics; GAFF, Generalized Amber Force Field; EM, Energy minimization; PME, particle mesh Ewald; RMSD, root-mean-square deviation; Rg, radius of gyration; RMSF, root-mean-square fluctuation; SASA, solvent-accessible surface area; NVT, constant number of particles, volume, and temperature; NPT, constant number of particles, pressure, and temperature; BDNF, brain-derived neurotrophic factor; CKB, creatine kinase B; RESP, the restrained electrostatic potential.

Availability of Data and Materials

The datasets generated and analyzed during the current study, including raw experimental data, are available from the corresponding author upon reasonable request.

Author Contributions

YCL, LL and QM designed the research study. YCL, LL, QM, MHH, XFG and SYY performed the research. LJL, YC and DSZ provided help and advice on the experiments. LL analyzed the data. YCL drafted the manuscript. All authors contributed to critical revision of the manuscript for important intellectual content. All authors read and approved the final manuscript. All authors have participated sufficiently in the work and agreed to be accountable for all aspects of the work.

Ethics Approval and Consent to Participate

Not applicable.

Acknowledgment

Not applicable.

Funding

This research received no external funding.

Conflict of Interest

The authors declare no conflict of interest.

Declaration of AI and AI-Assisted Technologies in the Writing Process

During the preparation of this work the authors used ChatGpt-3.5 in order to check spell and grammar. After using this tool, the authors reviewed and edited the content as needed and takes full responsibility for the content of the publication.

References

[1] Campbell BC, De Silva DA, Macleod MR, Coutts SB, Schwamm LH, Davis SM, *et al*. Ischaemic stroke. Nature Reviews Disease Primers. 2019; 5: 70. https://doi.org/10.1038/s41572-019-0118-8.

[2] GBD 2021 Diseases and Injuries Collaborators. Global incidence, prevalence, years lived with disability (YLDs), disability-adjusted life-years (DALYs), and healthy life expectancy (HALE) for 371 diseases and injuries in 204 countries and territories and 811 subnational locations, 1990-2021: a systematic analysis for the Global Burden of Disease Study 2021. Lancet (London, England). 2024; 403: 2133–2161. https://doi.org/10.1016/S0140-6736(24)00757-8.

[3] Yin KJ, Hamblin M, Eugene Chen Y. Angiogenesis-regulating microRNAs and ischemic stroke. Current vascular pharmacology. 2015; 13: 352–365.

[4] Carmeliet P, Jain RK. Molecular mechanisms and clinical applications of angiogenesis. Nature. 2011; 473: 298–307. https://doi.org/10.1038/nature10144.

[5] Ruan L, Wang B, ZhuGe Q, Jin K. Coupling of neurogenesis and angiogenesis after ischemic stroke. Brain Research. 2015; 1623: 166–173. https://doi.org/10.1016/j.brainres.2015.02.042.

[6] Chen D, Wei L, Liu ZR, Yang JJ, Gu X, Wei ZZ, *et al*. Pyruvate Kinase M2 Increases Angiogenesis, Neurogenesis, and Functional Recovery Mediated by Upregulation of STAT3 and Focal Adhesion Kinase Activities After Ischemic Stroke in Adult Mice. Neurotherapeutics: the Journal of the American Society for Experimental NeuroTherapeutics. 2018; 15: 770–784. https://doi.org/10.1007/s13311-018-0635-2.

[7] Hoffmann CJ, Harms U, Rex A, Szulzewsky F, Wolf SA, Grittner U, *et al*. Vascular signal transducer and activator of transcription-3 promotes angiogenesis and neuroplasticity long-term after stroke. Circulation. 2015; 131: 1772–1782. https://doi.org/10.1161/CIRCULATIONAHA.114.013003.

[8] Zhang W, Wang H, Zhang H, Leak RK, Shi Y, Hu X, *et al*. Dietary supplementation with omega-3 polyunsaturated fatty acids robustly promotes neurovascular restorative dynamics and improves neurological functions after stroke. Experimental Neurology. 2015; 272: 170–180. https://doi.org/10.1016/j.expneurol.2015.03.005.

[9] Kanazawa M, Takahashi T, Ishikawa M, Onodera O, Shimohata T, Del Zoppo GJ. Angiogenesis in the ischemic core: A potential treatment target? Journal of Cerebral Blood Flow and Metabolism: Official Journal of the International Society of Cerebral Blood Flow and Metabolism. 2019; 39: 753–769. https://doi.org/10.1177/0271678X19834158.

[10] Slevin M, Kumar P, Gaffney J, Kumar S, Krupinski J. Can angiogenesis be exploited to improve stroke outcome? Mechanisms and therapeutic potential. Clinical Science (London, England: 1979). 2006; 111: 171–183. https://doi.org/10.1042/CS20060049.

[11] Zhang Y, Liu L, Zhao X, Yan S, Zeng F, Zhou D. New insight into ischemic stroke: Circadian rhythm in post-stroke angiogenesis. Frontiers in Pharmacology. 2022; 13: 927506. https://doi.org/10.3389/fphar.2022.927506.

[12] Arkelius K, Wendt TS, Andersson H, Arnou A, Gottschalk M, Gonzales RJ, *et al*. LOX-1 and MMP-9 Inhibition Attenuates the Detrimental Effects of Delayed rt-PA Therapy and Improves Outcomes After Acute Ischemic Stroke. Circulation Research. 2024; 134: 954–969. https://doi.org/10.1161/CIRCRESAHA.123.323371.

[13] Geng YQ, Qiu LN, Cheng YQ, Li JJ, Ma YL, Zhao CC, *et al*. Alleviating Recombinant Tissue Plasminogen Activator-induced Hemorrhagic Transformation in Ischemic Stroke via Targeted Delivery of a Ferroptosis Inhibitor. Advanced Science (Weinheim, Baden-Wurttemberg, Germany). 2024; 11: e2309517. https://doi.org/10.1002/advs.202309517.

[14] Cao Y, Yang L, Cheng H. Ginkgolide B Protects Against Ischemic Stroke *via* Targeting AMPK/PINK1. Frontiers in Pharmacology. 2022; 13: 941094. https://doi.org/10.3389/fphar.2022.941094.

[15] Fang W, Deng Y, Li Y, Shang E, Fang F, Lv P, *et al*. Blood brain barrier permeability and therapeutic time window of Ginkgolide B in ischemia-reperfusion injury. European Journal of Pharmaceutical Sciences: Official Journal of the European Federation for Pharmaceutical Sciences. 2010; 39: 8–14. https://doi.org/10.1016/j.ejps.2009.10.002.

[16] Wang J, Zhuang L, Ding Y, Wang Z, Xiao W, Zhu J. A RNA-seq approach for exploring the protective effect of ginkgolide B on glutamate-induced astrocytes injury. Journal of Ethnopharmacology. 2021; 270: 113807. https://doi.org/10.1016/j.jep.2021.113807.

[17] Feng Z, Sun Q, Chen W, Bai Y, Hu D, Xie X. The neuroprotective mechanisms of ginkgolides and bilobalide in cerebral ischemic injury: a literature review. Molecular Medicine (Cambridge, Mass.). 2019; 25: 57. https://doi.org/10.1186/s10020-019-0125-y.

[18] Gu X, Xie Z, Wang Q, Liu G, Qu Y, Zhang L, *et al*. Transcriptome profiling analysis reveals multiple modulatory effects of Ginkgo biloba extract in the liver of rats on a high-fat diet. The FEBS Journal. 2009; 276: 1450–1458. https://doi.org/10.1111/j.1742-4658.2009.06886.x.

[19] Ke J, Li MT, Huo YJ, Cheng YQ, Guo SF, Wu Y, *et al*. The Synergistic Effect of *Ginkgo biloba* Extract 50 and Aspirin Against Platelet Aggregation. Drug Design, Development and Therapy. 2021; 15: 3543–3560. https://doi.org/10.2147/DDDT.S318515.

[20] Liang W, Yang H, Pan L, Wei S, Li Z, Zhang P, *et al*. Ginkgo biloba Extract 50 (GBE50) Exerts Antifibrotic and Antioxidant Effects on Pulmonary Fibrosis in Mice by Regulating Nrf2 and TGF-β1/Smad Pathways. Applied Biochemistry and Biotechnology. 2024; 196: 4807–4822. https://doi.org/10.1007/s12010-023-04755-9.

[21] Lu S, Guo X, Zhao P. Effect of Ginkgo biloba extract 50 on immunity and antioxidant enzyme activities in ischemia reperfusion rats. Molecules (Basel, Switzerland). 2011; 16: 9194–9206. https://doi.org/10.3390/molecules16119194.

[22] Wu Y, Li Z, Ding T, Yang Y, Wei C, Zhang S, *et al*. Bidirectional regulation of neuronal autophagy in ischemic stroke: Mechanisms and therapeutic potential. Ageing Research Reviews. 2025; 111: 102842. https://doi.org/10.1016/j.arr.2025.102842.

[23] Zou R, Liu Z, Wang P, Liu Y. Ginkgolide B binds to GPX4 and FSP1 to alleviate cerebral ischemia/reperfusion injury in rats. Toxicology and Applied Pharmacology. 2025; 495: 117237. https://doi.org/10.1016/j.taap.2025.117237.

[24] Liu H, Lei W, Ren Y, Tian J, Wang D, Tang Y, *et al*. Protective effects of Ginkgolide B on myocardial ischemia reperfusion injury: role of the GAS6/Axl signaling pathway. Chemico-biological Interactions. 2025; 418: 111607. https://doi.org/10.1016/j.cbi.2025.111607.

[25] Liang JH, Yu H, Xia CP, Zheng YH, Zhang Z, Chen Y, *et al*. Ginkgolide B effectively mitigates neuropathic pain by suppressing the activation of the NLRP3 inflammasome through the induction of mitophagy in rats. Biomedicine & Pharmacotherapy = Biomedecine & Pharmacotherapie. 2024; 177: 117006. https://doi.org/10.1016/j.biopha.2024.117006.

[26] Lee CW, Wang BYH, Wong SH, Chen YF, Cao Q, Hsiao AWT, *et al*. Ginkgolide B increases healthspan and lifespan of female mice. Nature Aging. 2025; 5: 237–258. https://doi.org/10.1038/s43587-024-00802-0.

[27] Hu C, Hu T, Wen J, Jia Z. Human papillomavirus-related syntaxin 11 reprograms tumor-associated macrophages to induce breast cancer cell apoptosis via PI3K/AKT signaling. Molecu-

lar Medicine (Cambridge, Mass.). 2025; 31: 285. https://doi.org/10.1186/s10020-025-01325-z.

[28] Wang K, He M, Tan Z, Tang X, Du B, Li P. Arabinogalactan polysaccharides derived from sacha inchi shells alleviate angiotensin II-induced endothelial cell dysfunction. Carbohydrate Polymers. 2025; 368: 124149. https://doi.org/10.1016/j.carbpol.2025.124149.

[29] Su D, Cheng F, Jiang Q, Zhang Y, Du F, Pan C, *et al*. Preconditioning With TGF-β Inhibitors Enhances Therapeutic Efficacy of Endothelial Progenitor Cells for Wound Healing in Diabetic Mice. MedComm. 2025; 6: e70364. https://doi.org/10.1002/mco2.70364.

[30] Sun J, Huang X, Zeng X, Lei Y, He H, Wei Z, *et al*. DBN1 mediated upregulation of GAB2 facilitates the migration and invasion of T cell acute lymphoblastic leukemia cells. Oncology Reports. 2025; 54: 149. https://doi.org/10.3892/or.2025.8982.

[31] Wang N, Wei X, Zhou P, Wu W, Liu J, Zhu H, *et al*. Palmatine mitigates ischemic brain injury by regulating microglial polarization and sphingolipid metabolism. International Immunopharmacology. 2025; 165: 115444. https://doi.org/10.1016/j.intimp.2025.115444.

[32] Ling S, Jin L, Li S, Zhang F, Xu Q, Liu M, *et al*. *Allium macrostemon* Saponin Inhibits Activation of Platelet via the CD40 Signaling Pathway. Frontiers in Pharmacology. 2021; 11: 570603. https://doi.org/10.3389/fphar.2020.570603.

[33] Wang JX, Xu XY, Dong HK, Wang YM, Dai M, Zhou B, *et al*. Exomeres From Adventitial Fibroblasts of Spontaneously Hypertensive Rats Promote Vascular Remodelling via Transferring Osteopontin. Journal of Extracellular Vesicles. 2025; 14: e70146. https://doi.org/10.1002/jev2.70146.

[34] Zhou PT, Wang LP, Qu MJ, Shen H, Zheng HR, Deng LD, *et al*. Dl-3-N-butylphthalide promotes angiogenesis and upregulates sonic hedgehog expression after cerebral ischemia in rats. CNS Neuroscience & Therapeutics. 2019; 25: 748–758. https://doi.org/10.1111/cns.13104.

[35] Liu Y, Yang X, Gan J, Chen S, Xiao ZX, Cao Y. CB-Dock2: improved protein-ligand blind docking by integrating cavity detection, docking and homologous template fitting. Nucleic Acids Research. 2022; 50: W159–W164. https://doi.org/10.1093/nar/gkac394.

[36] Luo J, Zhu Y, Yu Y, Chen Y, He K, Liu J. Sinomenine treats rheumatoid arthritis by inhibiting MMP9 and inflammatory cytokines expression: bioinformatics analysis and experimental validation. Scientific Reports. 2024; 14: 12786. https://doi.org/10.1038/s41598-024-61769-x.

[37] Trott O, Olson AJ. AutoDock Vina: improving the speed and accuracy of docking with a new scoring function, efficient optimization, and multithreading. Journal of Computational Chemistry. 2010; 31: 455–461. https://doi.org/10.1002/jcc.21334.

[38] Abraham MJ, Murtola T, Schulz R, Páll S, Smith JC, Hess B, *et al*. GROMACS: High performance molecular simulations through multi-level parallelism from laptops to supercomputers. SoftwareX. 2015; 1: 19–25. https://doi.org/10.1016/j.softx.2015.06.001.

[39] Van Der Spoel D, Lindahl E, Hess B, Groenhof G, Mark AE, Berendsen HJ. GROMACS: fast, flexible, and free. Journal of Computational Chemistry. 2005; 26: 1701–1718. https://doi.org/10.1002/jcc.20291.

[40] Ning S, Zhang S, Guo Z. MicroRNA-494 regulates high glucose-induced cardiomyocyte apoptosis and autophagy by PI3K/AKT/mTOR signalling pathway. ESC Heart Failure. 2023; 10: 1401–1411. https://doi.org/10.1002/ehf2.14311.

[41] Sun H, Wang G, Ren C, Zhang X, Zhao P, Guo B. Erianin inhibits cell migration and induces apoptosis by inhibiting VEGF-α/PI3K/AKT signaling pathway in malignant melanoma. Scientific Reports. 2025; 15: 15766. https://doi.org/10.1038/s41598-025-99383-0.

[42] Yun Z, Wu J, Sun X, Yu T, Xue W, Dai A, *et al*. Neural-enhancing PRP/Alg/GelMA triple-network hydrogel for neurogenesis and angiogenesis after spinal cord injury via PI3K/AKT/mTOR signaling pathway. Theranostics. 2025; 15: 3837–3861. https://doi.org/10.7150/thno.109091.

[43] Du J, Zhang L, Wang Z, Yano N, Zhao YT, Wei L, *et al*. Exendin-4 induces myocardial protection through MKK3 and Akt-1 in infarcted hearts. American Journal of Physiology. Cell Physiology. 2016; 310: C270–83. https://doi.org/10.1152/ajpcell.00194.2015.

[44] Li L, Yuan Y, Zhang C, Li Y, Xu R, Zhang X, Shang W. Melatonin Promotes Cerebral Angiogenesis in Ischemic Mice via BMP6/Smad1/5/9 Pathway. Molecular neurobiology. 2025, 62(9): 11362–11381. https://doi.org/10.1007/s12035-025-04969-4.

[45] Zhong S, Bai Z, Wu J, Wu M, Zhang RJZ, Lai R, *et al*. Static Magnetic Field Accelerates Wound Healing by Activation PI3K/AKT/mTOR Signaling Pathway. Current Medicinal Chemistry. 2025. https://doi.org/10.2174/0109298673379670250703084615. (online ahead of print)

[46] Cheng C, Liu H, Guan G, Fei Q, Zhao M, Wang H, *et al*. Yindan Xinnaotong Soft Capsule improves post-ischemic stroke recovery by regulating CREB/BDNF-mediated synaptic plasticity and CREB/VEGFA-mediated angiogenesis. Phytomedicine: International Journal of Phytotherapy and Phytopharmacology. 2025; 146: 157155. https://doi.org/10.1016/j.phymed.2025.157155.

[47] Li J, Stuhlmann H. In vitro imaging of angiogenesis using embryonic stem cell-derived endothelial cells. Stem Cells and Development. 2012; 21: 331–342. https://doi.org/10.1089/scd.2010.0587.

[48] Zhu T, Wang L, Wang LP, Wan Q. Therapeutic targets of neuroprotection and neurorestoration in ischemic stroke: Applications for natural compounds from medicinal herbs. Biomedicine & Pharmacotherapy = Biomedecine & Pharmacotherapie. 2022; 148: 112719. https://doi.org/10.1016/j.biopha.2022.112719.

[49] Wei XX, Tang XQ. Platelets: A new therapeutic target for neurological diseases. Ageing Research Reviews. 2025; 112: 102874. https://doi.org/10.1016/j.arr.2025.102874.

[50] Wei H, Sun T, Tian Y, Wang K. Ginkgolide B Modulates BDNF Expression in Acute Ischemic Stroke. Journal of Korean Neurosurgical Society. 2017; 60: 391–396. https://doi.org/10.3340/jkns.2016.1010.018.

[51] Yang K, Zeng L, Ge A, Chen Y, Wang S, Zhu X, *et al*. Exploring the Regulatory Mechanism of *Hedysarum Multijugum Maxim.-Chuanxiong Rhizoma* Compound on HIF-VEGF Pathway and Cerebral Ischemia-Reperfusion Injury's Biological Network Based on Systematic Pharmacology. Frontiers in Pharmacology. 2021; 12: 601846. https://doi.org/10.3389/fphar.2021.601846.

[52] Shu ZM, Shu XD, Li HQ, Sun Y, Shan H, Sun XY, *et al*. Ginkgolide B Protects Against Ischemic Stroke Via Modulating Microglia Polarization in Mice. CNS Neuroscience & Therapeutics. 2016; 22: 729–739. https://doi.org/10.1111/cns.12577.

[53] Zhu J, Jin Z, Yang L, Zhao C, Hu J, Chen J, *et al*. Ginkgolide B targets and inhibits creatine kinase B to regulate the CCT/TRiC-SK1 axis and exerts pro-angiogenic activity in middle cerebral artery occlusion mice. Pharmacological Research. 2022; 180: 106240. https://doi.org/10.1016/j.phrs.2022.106240.

[54] Liu Q, Jin Z, Xu Z, Yang H, Li L, Li G, *et al*. Antioxidant effects of ginkgolides and bilobalide against cerebral ischemia injury by activating the Akt/Nrf2 pathway in vitro and in vivo. Cell Stress & Chaperones. 2019; 24: 441–452. https://doi.org/10.1007/s12192-019-00977-1.